


Effect of deformation in the scattering and reaction of a ${}^9\text{C}$ radioactive beam by protons and ${}^{12}\text{C}$, and extraction of the density distribution of ${}^9\text{C}$

M. Rashdan, M. M. Taha , and M. A. El-Sayed*Mathematics and Theoretical Physics Department, NRC, Egyptian Atomic Energy Authority, 13759 Cairo, Egypt*

(Received 3 April 2023; accepted 29 June 2023; published 18 July 2023)

The effect of deformation in the scattering and reaction of a ${}^9\text{C}$ radioactive beam by protons and ${}^{12}\text{C}$ is investigated within the relativistic impulse approximation and a modified Glauber model whose amplitude involved the combined effects of phase variation, higher momentum transfer components, Pauli blocking, and finite range. Spherical and deformed relativistic mean field densities are used. Using the proton scattering experiment by ${}^9\text{C}$ as well as interaction cross section data, the proton and neutron root mean square (rms) radii and deformations are extracted. It is found that deformation strongly affects the scattering cross section and polarization at medium and large angles, where the second and third peaks are reproduced by a deformed density. The polarization is inverted at the peaks by deformation. The measured angular distribution of the proton by a ${}^9\text{C}$ beam at 277–300 MeV/u as well as the reaction cross section data of ${}^9\text{C} + {}^{12}\text{C}$ at 680 and 720 MeV/u are satisfactorily reproduced by an extracted deformed Woods-Saxon density of ${}^9\text{C}$ with matter rms radius and deformation parameter of the order $R_m \approx 2.33$ fm and $\beta_m \approx 0.36$.

DOI: [10.1103/PhysRevC.108.014607](https://doi.org/10.1103/PhysRevC.108.014607)

I. INTRODUCTION

Recent developments in the study of unstable nuclei have inspired renewed interest in nuclear radii and proton and neutron density distributions (for a recent review see, e.g., Refs. [1–4]). Proton elastic scattering at intermediate energies is one way for examining these distributions. We can directly compare proton elastic scattering with nuclear density distributions using a relativistic impulse approximation (RIA) [5–13] or a folding model with g -matrix interaction [14]. In the RIA the motion of the projectile in the field of the nucleus is described with the relativistic Dirac equation that describes the interacting nucleons via meson exchanges. It has the advantage that the spin-orbit interaction is built in without any need for adjustable parameters. It also has provided a remarkably good description of the elastic cross section and spin observable at intermediate and high energies [5–13].

The aim of the present work is to use the RIA to study p - ${}^9\text{C}$ scattering at intermediate energy. The study of p - ${}^9\text{C}$ scattering is very interesting and important for knowing the properties of a proton-nucleon interaction with a few-body system. Among the carbon isotopes, ${}^9\text{C}$ is a nucleus of interest that is near the proton drip-line. The measurement of the differential elastic scattering of ${}^9\text{C}$ from protons at 277–300 MeV/nucleon has been reported by Matsuda *et al.* [15]. To obtain the nucleon distributions in ${}^9\text{C}$, they analyzed the experimental data by using spherical two-parameters Fermi (2pF) distribution for protons and neutrons. In addition, they assumed density dependence coupling constants and meson masses in terms of four parameters in the NN -scattering amplitudes. With these additional four parameters in the NN -scattering amplitudes and the other four parameters of the spherical (two for proton and two neutrons) Fermi densities Matsuda *et al.* were able

to fit the proton- ${}^9\text{C}$ differential elastic cross section data but with highly unphysical deduced proton and neutron density distributions.

In view of the failure of the method of Matsuda *et al.* to yield reasonable proton and neutron distributions, Rafi *et al.* [16] had reanalyzed the measured proton- ${}^9\text{C}$ elastic angular distribution within the Brueckner-Hartree-Fock framework using the Argonne v-18 internucleon potential and density distributions obtained from a spherical relativistic mean-field (RMF) calculation. The calculations yield a good agreement with the experimental data up to angle 30 (degrees). The second peak in the data after 30 (degrees) cannot be described by Rafi *et al.* where they get a decrease of steeper slope at 30° like that obtained by the original RIA when using spherical RMF densities (see Fig. (10) of [15]). In fact, nuclear structure calculations predicted ${}^9\text{C}$ to be strongly deformed. Thus assuming ${}^9\text{C}$ has spherical densities, as Matsuda *et al.* and Rafi *et al.* had done, is a crude approximation.

In this work, we investigate the effect of deformation in the scattering of ${}^9\text{C}$ radioactive beams by protons at intermediate energy within the RIA as well as in the reaction cross section of ${}^9\text{C} + {}^{12}\text{C}$ at high energy using a modified Glauber model whose amplitude involved combining effects of phase variation, higher momentum transfer components, Pauli blocking, and finite range. Furthermore, we extract the density distribution of ${}^9\text{C}$. Section II presents the theoretical description. The results are presented and discussed in Sec. III.

II. THEORETICAL DESCRIPTION

In the relativistic impulse approximation the Dirac equation for the single-particle motion of the projectile nucleon in

TABLE I. The spherical and deformed RMF radii and deformation parameters of ${}^9\text{C}$ calculated using NLRA1 interaction.

R_n^s (fm)	R_p^s (fm)	R_m^s (fm)	R_n^d (fm)	R_p^d (fm)	R_m^d (fm)	β_{2n}	β_{2p}	β_{2m}
1.976	2.58	2.395	2.195	2.710	2.550	0.4194	0.3930	0.4018

the mean field of the target nucleus can be written as [5–13]

$$[-i\alpha\nabla + U_V(r; E) + \beta(M + U_S(r; E)) + V_C]|\psi\rangle = E|\psi\rangle, \quad (1)$$

where U_S and U_V are the scalar and vector potentials which contain both direct and exchange parts,

$$U_{L(=S,V)} \equiv U_L^D(r; E) + U_L^X(r; E). \quad (2)$$

E is the total nucleon-nucleus center of mass (c.m.) projectile energy, M is its rest mass, and V_C is the Coulomb potential energy. The Dirac optical potentials are calculated from the nucleon-nucleon (NN) t matrix, where the action of these potentials on the incident projectile wave function, projected in the coordinate space, can be written as

$$\begin{aligned} \langle x|U_{\text{opt}}|\psi_0\rangle &= -\frac{4\pi ip}{M} \sum_{\alpha}^{\text{occ}} \int d^3y' \int d^3y \int d^3x' \overline{\psi}_{\alpha} \\ &\times [\langle xy'|t(E)|x'y\rangle + (-1)^T \langle y'x|t(E)|x'y\rangle] \\ &\times \psi_0(x')\psi_{\alpha}(y), \end{aligned} \quad (3)$$

where

$$U_{\text{opt}} = U_S + \gamma^0 U_V. \quad (4)$$

p is the magnitude of the three-momentum of the projectile in the nucleon-nucleus c.m. frame and T is the total isospin of the two-nucleon state. The antisymmetrized matrix element of $t(E)$ in coordinate space is the Fourier transform of the momentum space matrix element. The t matrix $t(E)$ is the lowest-order meson-exchange diagram evaluated from the Feynman rules. The mesons have different spins and parities (scalar, vector, tensor, pseudoscalar, and axial vector) and isospin 0 and 1. The Dirac optical potentials (direct and exchange parts) are written as a folding integral of the nucleon-nucleon t matrix and the target (scalar and vector) densities:

$$U_L^D(r; E) = -\frac{4\pi ip}{M} \int d^3r' \rho_L(\mathbf{r}') t_L^D(|\mathbf{r} - \mathbf{r}'|; E), \quad (5)$$

$$\begin{aligned} U_L^X(r; E) &= -\frac{4\pi ip}{M} \int d^3r' \rho_L(\mathbf{r}, \mathbf{r}') t_L^X(|\mathbf{r} - \mathbf{r}'|; E) j_0 \\ &\times \left(\frac{p}{\hbar} |\mathbf{r} - \mathbf{r}'| \right), \end{aligned} \quad (6)$$

where the local density approximation is used for the nonlocal exchange term and

$$t_L^{D,X}(s; E) = \int \frac{d^3q}{2\pi^3} t_L^{D,X}(\mathbf{q}; E) e^{-i\mathbf{q}\cdot\mathbf{s}}. \quad (7)$$

The off-diagonal density matrix $\rho_L(\mathbf{r}, \mathbf{r}')$ is approximated to be given in terms of the one-body densities, using the density matrix expansion approximation. For the NN t matrix we used the parametrization of [11–13]. For laboratory energies

≈ 200 – 500 MeV, the Dirac optical potentials are modified by a Pauling blocking low energy correction [12,13].

III. RESULTS AND DISCUSSION

For the projectile ${}^9\text{C}$ a modified deformed Fermi distribution is considered for protons and neutrons in which both radii and diffuseness are depend on deformations,

$$\rho_{i=p,n}(\mathbf{r}) = \frac{\rho_{0i}}{1 + \exp\left(\frac{r - R_i(\theta)}{a_i(\theta)}\right)}, \quad (8)$$

where

$$R_i(\theta) = R_{0i}[1 + \beta_{2i}Y_{20}(\theta)]. \quad (9)$$

The expansion (9) is a well familiar approximation of the deformed half-density radius. The diffuseness is also assumed to depend on deformation and can be expanded in a similar way to the radius as

$$a_i(\theta) = a_{0i}[1 + \beta_{2i}Y_{20}(\theta)]. \quad (10)$$

The advantage of introducing a deformed diffuseness parameter in the Fermi shape is to increase the dependence of the density distribution on the deformation parameters.

The angle-average approximation is used [17,18]:

$$\rho(r) = \frac{1}{2} \int_0^{\pi} \rho(r, \theta) \sin(\theta) d\theta. \quad (11)$$

The quadrupole deformation parameters and root mean square (rms) radii for protons and neutrons can be determined by deformed RMF calculations, using the number of boson and fermion shells ($n_B = n_F = 12$) [19], and they are listed in Table I. The neutron diffuseness parameter a_{0n} is assumed to depend on the asymmetry $(N - Z)/A$ as $a_{0n} = a_{0p} + a_s(N - Z)/A$, where a_{0p} is the proton diffuseness parameter. For a deformed-average (def-av.) RMF density a_{0p} is fixed to 0.4 fm and a_s to 0.222 fm and the half-density radii R_{0p} and R_{0n} are adjusted in order to reproduce the RMF rms proton and neutron radii.

The elastic scattering cross sections and polarization of p - ${}^9\text{C}$ at 200, 280, and 360 MeV calculated by the RIA using spherical and deformed averages. RMF densities are presented in Figs. 1, 2, and 3, denoted by short-dashed and dash double-dotted lines. For the deformed average scalar densities we used the approximation, $\rho_{ps} = \rho_p$ and $\rho_{ns} = \rho_n$ [20]. The NLRA1 interaction [21] is used in both spherical and deformed RMF calculations. Pairing is treated in the Bardeen-Cooper-Schrieffer (BCS) approximation using the model described in [22–24] for an energy gap of protons and neutrons. As shown from these figures the effect of deformation is to make the second and third (see Fig. 3) peaks and minima well defined and shifted to smaller angles. The well-defined peak appearing at large angles by the deformed density totally disappears by using a spherical RMF density.

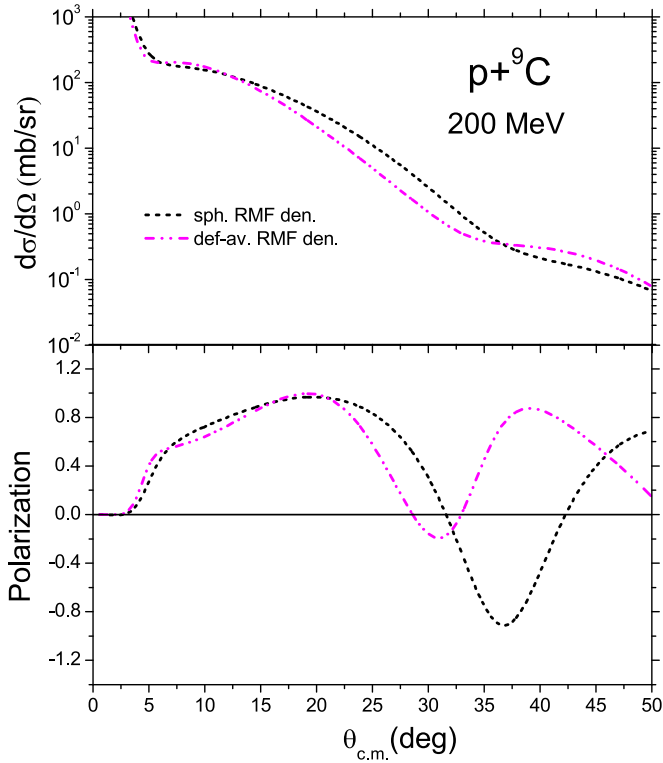


FIG. 1. The elastic scattering cross section and polarization of $p + {}^9\text{C}$ at E_{lab} at 200 MeV.

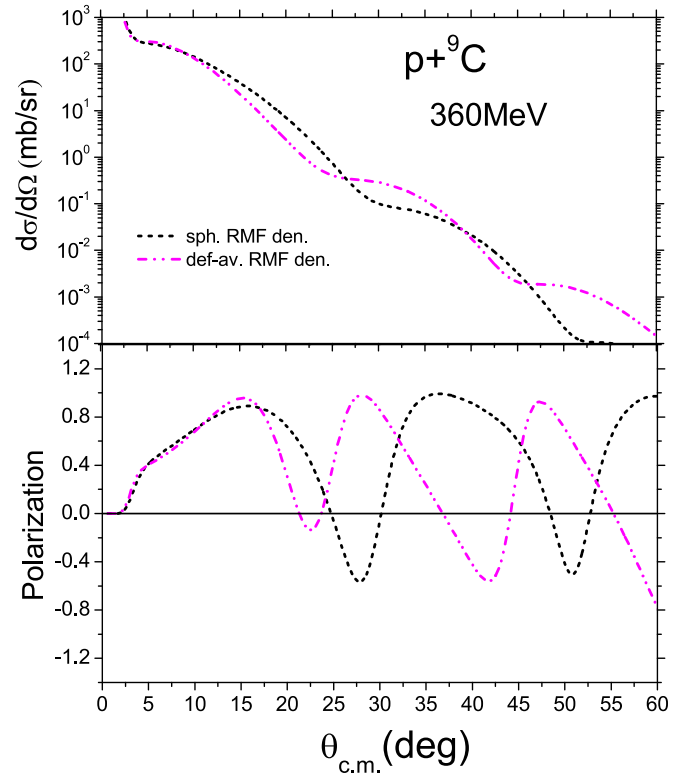


FIG. 3. Same as Fig. 1 but at 360 MeV.

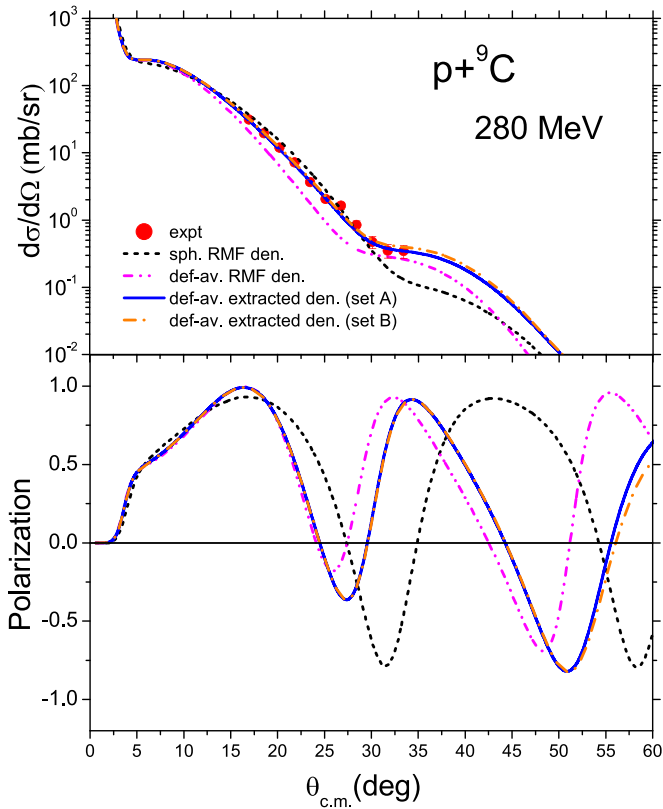


FIG. 2. The elastic scattering cross section and polarization of $p + {}^9\text{C}$ at E_{lab} at 280 MeV in comparison with the data at 277–300 MeV.

The polarization is strongly affected by deformation where it has an inverse behavior at the peaks in the cross section, as shown from Figs. 1–3. Although the deformed density well defined the peaks in the cross section it presents lower a cross section than the data, as shown from Fig. 2, which could be due to the larger radii and deformation parameters predicted by RMF. On the other hand, Skyrme Hartree-Fock (SHF) calculations [25] predicted smaller deformations, and consequently smaller rms radii, than those of the RMF calculation.

In order to fit the data at 277–300 MeV we scale the RMF proton and neutron deformed rms radii and deformation parameters, listed in Table I, by factors $c_{i(=p,n)}$ and c'_i as

$$R_{i(=p,n)} = c_i \times R_i^{\text{RMF}}, \quad \beta_{i(=p,n)} = c'_i \times \beta_i^{\text{RMF}}. \quad (12)$$

For simplicity, we assume $c'_i = c_i$. a_{0p} is fixed to 0.307 fm and a_s to 0.27 fm. The half-density radii R_{0p} and R_{0n} are adjusted in order to reproduce the scaled RMF rms proton and neutron radii, where the scaled parameters c_p and c_n , which produced the scaled rms radii and deformations, are slowly decreased in order to catch the data and they are found to be $c_p = 0.941$ and $c_n = 0.825$. The parameters of the extracted density distribution are listed in Table II, denoted by set A. The second row in Table II gives the parameters of the extracted proton and neutron densities but when using deformation parameters derived from deformed SHF calculations [25]. The other parameters of the density distributions, like the half-density radii and diffuseness, are fixed to those of set A. The SHF deformation parameters are smaller than those of the RMF and those extracted in set A, thus they have predicted smaller rms radii, as seen from Table II. The extracted proton,

TABLE II. The extracted proton and neutron deformed WS density parameters and rms radii, denoted by sets A and B, which are described in the text.

set	R_{0p} (fm)	R_{0n} (fm)	a_{0p} (fm)	a_{0n} (fm)	β_p (fm)	β_n (fm)	β_m (fm)	R_p (fm)	R_n (fm)	R_m (fm)
A	2.8025	2.004	0.307	0.217	0.370	0.346	0.360	2.5500	1.8104	2.3300
B	2.8025	2.004	0.307	0.217	0.273	0.251	0.269	2.5055	1.7813	2.2897

neutron and total densities are plotted in Fig. 4, where set A produced slightly larger surface and tail regions, due to their larger deformations.

The elastic scattering cross section and polarization calculated by these extracted densities are plotted in Fig. 2 by solid (set A) and dash-dotted (set B) lines. As shown from this figure the extracted density set A satisfactorily reproduced the data at all angles. Set B can also well describe the data, although it predicted slightly higher cross sections at the second peak. The spherical RMF densities give much lower cross sections after 30° , where the second peak disappears as those obtained in [15,16] where they used spherical RMF densities.

Figure 2 (lower part) shows a dramatic dependence of polarization on deformation, especially at medium and larger angles. For example, the first dip in the polarization calculated by spherical RMF density occurs at angle $\theta \cong 32.5^\circ$, while it is shifted to lower angles by deformation, where it occurs at

angle $\theta \cong 27.5^\circ$ by the extracted deformed density. Another important note is that this first dip is deeper when using a spherical RMF density, while it is diminished by deformation. It is also found that the second maximum in the polarization calculated by deformed extracted density occurs at $\theta \approx 34^\circ$, which nearly corresponds to the second maximum in the experimental differential cross section. On the other hand, the spherical RMF density presented an inverse behavior and shifted the second maximum in the polarization to a much larger angle, $\theta \approx 43^\circ$. Thus, data for polarization are of great important and are essentially needed in order to extract information about the density distribution of exotic nuclei.

Figure 5 shows the extracted densities (set A) in comparison with the spherical RMF densities as well as the spherical densities extracted by Matsuda *et al.* As shown from Fig. 5 (lower part) the extracted total def-av. density has larger surface and diffuseness than that of the spherical RMF density.

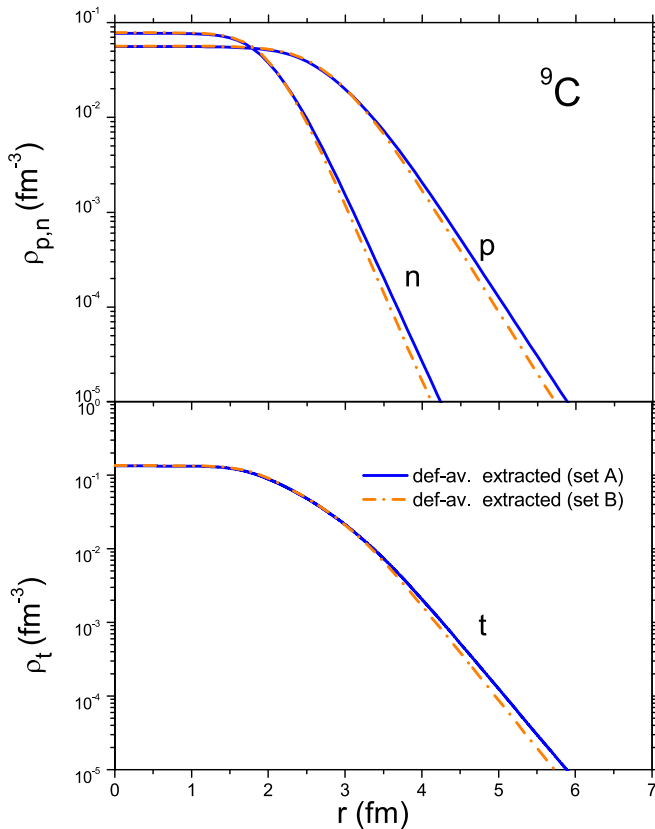


FIG. 4. The extracted def-av. proton and neutron (upper part) and total (lower part) density distributions by the present work, whose parameters are listed in Table II.

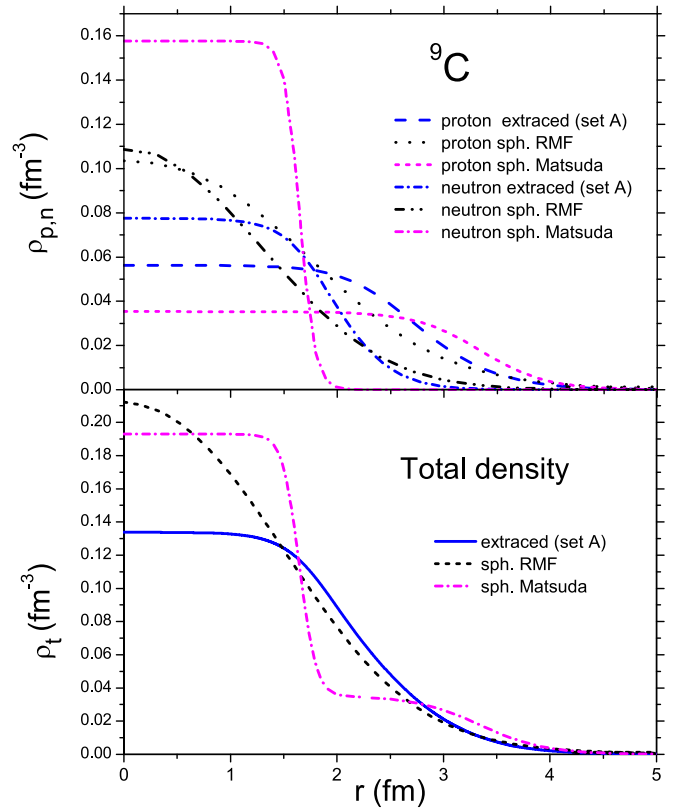


FIG. 5. The extracted def-av. proton and neutron (upper part) and total (lower part) density distributions by the present work (set A) in a comparison with the spherical RMF and those extracted by Matsuda *et al.* [15].

TABLE III. The reaction cross sections at 680 and 720 MeV/u calculated by parameter sets A and B in comparison with data [27]. The percentage errors (PE) are also listed, where $PE = \frac{|\sigma_R^{ex} - \sigma_R^{cal}|}{\sigma_R^{ex}} \times 100$.

set	$\sigma_R(680)$ (mb)	$\sigma_R^{ex}(680)$ (mb)	PE	$\sigma_R(720)$ (mb)	$\sigma_R^{ex}(720)$ (mb)	PE
A	815.4	812±13[27]	0.4	831.3	834±18[27]	0.3
B	796.0		2.0	813.9		2.4

This increases and modifies the cross section at large angles consistent with the data. The RMF densities give larger rms radii which is due to its much larger volume parts, as seen from Fig. 5. In comparison with Matsuda *et al.* we found the present extracted def-av. Woods-Saxon (WS) density is more reliable and physical than the spherical WS density extracted

by Matsuda *et al.*, which is highly unphysical and contradicts with experiments as well as nuclear structure predictions.

In order to examine the extracted densities for reaction cross section data we calculated the reaction cross section of ${}^9\text{C} + {}^{12}\text{C}$ at 680 and 720 MeV/u, using a modified Glauber model, which involves the combined effect of the phase variation, higher momentum transfer components, and Pauli blocking of the NN amplitude [26]. We get the results listed in Table III. As seen from this table, set A satisfactorily produced the reaction cross section data [27] and has much smaller percentage errors which are of the order of 0.3–0.4%. Set B has much larger percentage errors than set A, as seen from Table II. This also favors the present extracted deformation parameters and radii of set A in describing ${}^9\text{C}$.

Finally, one can conclude that both the elastic scattering and the reaction cross section experiments are important in order to extract more reliable information about the radii and densities of neutron or proton-rich nuclei.

-
- [1] T. Otsuka, A. Gade, O. Sorlin, T. Suzuki, and Y. Utsuno, *Rev. Mod. Phys.* **92**, 015002 (2020).
- [2] T. Nakamura, T. Sakurai, and H. Watanabe, *Prog. Part. Nucl. Phys.* **97**, 53 (2017).
- [3] P. Campbell, I. Moore, and M. Pearson, *Prog. Part. Nucl. Phys.* **86**, 127 (2016).
- [4] N. Shimizu, T. Abe, Y. Tsunoda, Y. Utsuno, T. Yoshida, T. Mizusaki, M. Honma, and T. Otsuka, *Prog. Theor. Exp. Phys.* **2012**, 01A205 (2012).
- [5] J. A. McNeil, J. R. Shepard, and S. J. Wallace, *Phys. Rev. Lett.* **50**, 1439 (1983).
- [6] J. R. Shepard, J. A. McNeil, and S. J. Wallace, *Phys. Rev. Lett.* **50**, 1443 (1983).
- [7] B. C. Clark, S. Hama, R. L. Mercer, L. Ray, and B. D. Serot, *Phys. Rev. Lett.* **50**, 1644 (1983).
- [8] B. C. Clark, S. Hama, R. L. Mercer, L. Ray, G. W. Hoffmann, and B. D. Serot, *Phys. Rev. C* **28**, 1421 (1983).
- [9] B. C. Clark, S. Hama, and R. L. Mercer, in *Workshop on the Interaction Between Medium-Energy Nucleons in Nuclei, 28–30 Oct. 1982, Bloomington, IN, USA*, edited by H. O. Meyer, *AIP Conf. Proc. No. 97* (AIP, New York, 1983), pp. 260–287.
- [10] J. A. Tjon and S. J. Wallace, *Phys. Rev. C* **32**, 1667 (1985).
- [11] C. J. Horowitz, *Phys. Rev. C* **31**, 1340 (1985).
- [12] D. P. Murdock and C. J. Horowitz, *Phys. Rev. C* **35**, 1442 (1987).
- [13] L. Ray, G. W. Hoffmann, and W. R. Coker, *Phys. Rep.* **212**, 223 (1992).
- [14] K. Amos, P. J. Dortmans, S. Karataglidis, H. V. von Geramb, and J. Raynal, in *Advances in Nuclear Physics*, edited by J. W. Negele and E. Vogt, (Kluwer Academic Publishers, New York, Boston, Dordrecht, London, Moscow, 2000), Vol. 25, p. 276.
- [15] Y. Matsuda *et al.*, *Phys. Rev. C* **87**, 034614 (2013).
- [16] S. Rafi, A. Bhagwat, W. Haider, and Y. K. Gambhir, *Phys. Rev. C* **89**, 067601 (2014).
- [17] K. Minomo, T. Sumi, M. Kimura, K. Ogata, Y. R. Shimizu, and M. Yahiro, *Phys. Rev. C* **84**, 034602 (2011).
- [18] M. Rashdan and Sh. Sewailem, *Phys. Rev. C* **99**, 034604 (2019).
- [19] M. Rashdan, *Int. J. Mod. Phys. E* **21**, 1250055 (2012).
- [20] M. Rashdan, *Eur. Phys. J. A* **16**, 371 (2003).
- [21] M. Rashdan, *Phys. Rev. C* **63**, 044303 (2001);
- [22] M. K. Sharma, M. S. Mehta, and S. K. Patra, *Int. J. Mod. Phys. E* **22**, 1350005 (2013).
- [23] D. G. Madland and J. R. Nix, *Nucl. Phys. A* **476**, 1 (1988).
- [24] P. Möller and J. R. Nix, *At. Data Nucl. Data Tables* **39**, 213 (1988).
- [25] H. Sagawa, X. R. Zhou, X. Z. Zhang, and T. Suzuki, *Phys. Rev. C* **70**, 054316 (2004).
- [26] S. Ahmad, A. A. Usmani, Sh. Ahmad, and Z. A. Khan, *Phys. Rev. C* **95**, 054601 (2017).
- [27] A. Ozawa, T. Suzuki, and I. Tanihata, *Nucl. Phys. A* **693**, 32 (2001).